State Estimation for Distribution Grids with a Single Point Grounded Neutral Conductor

Andreas Kotsonias, *Student Member, IEEE*, Markos Asprou, *Member, IEEE,*
Lenos Hadjidemetriou, *Member, IEEE,* and Elias Kyriakides, *Senior Member, IEEE*

Dedicated to the memory of Elias Kyriakides.

***Abstract*—Distribution system state estimation (DSSE) has been enabled by the deployment of smart meters and is currently the subject of active research, focused mainly in medium voltage distribution grids (MVDGs). This paper proposes a modified weighted least squares (WLS) DSSE for low voltage distribution grids (LVDGs) where the neutral conductor is grounded only at the MV-LV substation. DSSE methods developed for MVDGs are not applicable in such systems due to the significant voltage drop across the neutral conductor. The proposed DSSE includes the neutral voltage in the state vector and the measurement functions are modified accordingly. To address any convergence issues and to enhance the accuracy of the proposed DSSE, virtual measurements are introduced for the neutral voltage. The effectiveness of the proposed DSSE is illustrated in a real LVDG and in the IEEE European low voltage test feeder under different operating conditions, smart meter classes and system layouts. In addition, a Monte Carlo analysis is performed for highlighting the importance of the proposed modifications to the WLS DSSE. Among others the analysis indicate that the proposed method converged in all trials, despite including the neutral voltage in the state vector.**

***Index Terms*—Low voltage distribution grids, monitoring, neutral conductor, state estimation, weighted least squares.**

I. Introduction

LOW voltage distribution grids are entering a new era in which their role in the envisioned cost effective and sustainable power system is very important. The increasing penetration of distributed energy resources and the impending electrification of the transportation sector are transforming LVDGs into active and complex systems. During, as well as in the aftermath of this transition, several new challenges can arise where coordination and control strategies will be required in order to maintain the secure and efficient operation of the grid [1]. The functionalities of a distribution management system, such as alarms in case of detecting thermal constraints or voltage limits violations, the detection of fault location, demand side management and self-healing actions are all enabled by the DSSE. However, there are a number of challenges regarding the deployment of DSSE [2]-[3]. One of the main limiting factors for its deployment was, until very recently, the scarcity of measurement devices in the distribution system. This has been mitigated by the rapid growth of advanced metering infrastructure with a massive deployment of smart meters [4]. By utilizing these devices, the effective operation of the DSSE has been enabled and numerous works have been proposed.

Due to the different characteristics compared to the transmission system, the monitoring methods developed for transmission system cannot be applied directly to the DSSE. Considering that the most common transformer configuration in MV-LV substations is D-Y_g, the zero-sequence component of the asymmetrical currents introduced by the LVDG loads is eliminated at the substation and does not propagate into the MVDG. Consequently, the current flow in the neutral conductor of MVDGs is negligible, especially if it's multi-grounded, and the voltage drop across it can be approximated to zero. This allows the use of Kron's reduction [5]-[6], which reduces the size of the impedance matrix of each distribution line and the total number of state variables. In order to account for these characteristics, a three-phase coupled WLS DSSE is proposed in [5] where a three-phase, four-wire, multi-grounded system is simplified by using Kron's reduction. A branch-current (BC) DSSE is presented in [7] where both non-synchronized and synchronized measurements are considered. The proposed estimator is expressed in both polar and rectangular coordinates and can handle both radial and weekly meshed grids. In [8], a DSSE is presented which can handle voltage drop regulators, tap-changing transformers and a number of different type of measurements by introducing new equality constraints in the WLS DSSE procedure. The time skewness of the smart meter measurements is addressed in [9] by proposing a new method to adjust the variance and mean of each measurement. This method significantly improves the accuracy of the traditional DSSE [5] where the asynchronicity of the smart meter measurements is not considered. In [10], a two-step multi-area DSSE is presented. In the first step, a BC-DSSE is executed using local and shared measurements in each area. Then during the second step, a modified version of the WLS SE is used to refine the voltage profile estimation. The performance of a three-phase DSSE is evaluated in [11] under different types of knowledge, input data and measurement error models. The authors highlight the significance of not only having accurate measurements but also a good knowledge of

This work is supported by the European Regional Development Fund and the Republic of Cyprus through the Research and Innovation Foundation (Project: INTEGRATED/0916/0035). It is also supported by the European Union's Horizon 2020 research and innovation programme under grant agreement No 739551 (KIOS CoE) and from the Government of the Republic of Cyprus through the Directorate General for European Programmes, Coordination and Development.

A. Kotsonias, M. Asprou, and L. Hadjidemetriou are with the KIOS Research and Innovation Center of Excellence and the Department of Electrical and Computer Engineering, University of Cyprus, 1678 Nicosia, Cyprus (e-mail: kotsonias.andreas@ucy.ac.cy, asprou.markos@ucy.ac.cy, lhadji02@ucy.ac.cy).

E. Kyriakides, deceased, was with the Department of Electrical and Computer Engineering and KIOS Research Center of Excellence, University of Cyprus, 1678 Nicosia, Cyprus.

the system (layout and grid parameters). In [12], the DSSE of the MVDG is enhanced by exploiting the smart meters in the LVDGs. A multilevel DSSE is first used to determine the state of the LVDG. The estimated voltage and power flow at the MV-LV substation are then used as measurements in the MVDG DSSE. This method achieves full observability of the MVDG by exploiting the smart meters of the end-users without requiring additional measurement equipment. A DSSE for a four-wire MVDG composed of only grounded-wye loads where the neutral conductor is grounded at each system bus through a 1 Ohm grounding impedance is proposed in [13]. This formulation allows to eliminate the state variables corresponding to the neutral and zero-injection phase voltages which enhances the overall computational performance.

Most of the aforementioned works regarding the DSSE are under the assumption of a multi-grounded neutral conductor. While this is a valid assumption for most MVDGs, for LVDGs this may not be true. In fact, in Cyprus and in many other countries the neutral conductor in a LVDG is only grounded at the MV-LV substation. If such a DSSE is used in this kind of LVDGs, then a significant error is imposed on the estimation results [14]. The main reasons for this are: (1) the inaccurate system model due to the Kron's reduction and (2) the phase-to-neutral voltage measurements. Since the neutral voltage in these LVDGs is not insignificant and can vary considerably across the system, each voltage measurement is expressed with a different reference. This paper aims to address these issues with the following contributions: (1) a modified WLS SE where the neutral voltage is included in the state vector and the measurement functions are adjusted accordingly, (2) to address any potential convergence issues by including the neutral voltage in the WLS SE procedure, virtual measurements are constructed and (3) two fitness tests are conducted in order to verify the distribution of the virtual measurements' error and a mathematical calculation of their uncertainty (weighting scheme) is developed so that they are properly incorporated in the WLS SE procedure.

The remainder of this paper is organized as follows. In Section II the considered smart meters in the case studies are presented. The proposed modifications to the WLS SE are presented in Section III. In Section IV, the distribution of the virtual measurements is verified, and their uncertainty is calculated. The performance evaluation of the proposed and traditional WLS SE (C_N) is presented in Section V and the paper concludes in Section VI.

II. Smart Metering Infrastructure

A smart metering system consists of four main elements: the smart metering device (smart meter), a data concentrator, a communication system and the control center [4]. In the recent years, millions of smart meters have been deployed globally and by 2022 it is expected that around 1000 million of these devices will be installed worldwide. The main reason of their commissioning by utility companies is for automatic billing purposes and in general for understanding customers' behavior which can aid in improving the system's operation. However, by utilizing the vast amount of new data related to the LVDG operation, new applications and functionalities can be enabled [15]. For instance, load analysis, load forecasting, load management, energy theft detection and monitoring of the LVDG are some of the applications that will be enabled by the smart meter data.

TABLE I
PERCENTAGE MAXIMUM ERROR LIMITS OF SMART METERS

Accuracy Class	$\cos(\theta) = 0.5\ lagging$		$\cos(\theta) = 1$	
	$0.1I_n \le I \le 0.2I_N$	$0.2I_n \le I \le I_{max}$	$0.1I_n \le I \le 0.2I_N$	$0.2I_n \le I \le I_{max}$
0.2s	±0.5%	±0.3%	±0.4%	±0.2%
0.5s	±1.0%	±0.6%	±1.0%	±0.5%
0.5	±1.3%	±0.8%	±1.0%	±0.5%
1	±1.5%	±1.0%	±1.5%	±1.0%
2	±2.5%	±2.0%	±2.5%	±2.0%

TABLE II
CONSIDERED SMART METER ACCURACY CLASSES

Case	Accuracy Class		
	P	Q	V
1	0.2s	0.2s	±0.1%
2	0.5s	0.5	±0.3%
3	0.5	1	±0.5%
4	1	2	±1.0%
5	2	2	±1.5%

In this paper, a DSSE for a specific type of LVDG is proposed which utilizes the existing smart meters of the end-users (system is fully observable). A typical smart meter can provide measurements of the active and reactive power consumption as well as phase-to-neutral voltage measurements at the point of connection (premises of the consumer). Each measurement is classified according to the accuracy class of the meter. Assuming directly connected smart meters (no instrument transformers between the smart meter and the circuit) the overall accuracy of the different smart meter classes for the power measurements is presented in Table I as a function of the load current and the power factor. In this paper, five different smart meter accuracy classes are considered in the case studies, as presented in Table II. The measurement error is modeled as [11],

$$z_{meas} = z_{true} + FS \cdot N\left(0, \sigma_{P,Q,|V|}\right) \tag{1.a}$$

where z_{true} is the true value of the measured variable, FS is the full scale meter reading associated with each type of measurement (9.2 kVA for the power measurements and 300 V for voltage measurements) and $\sigma_{P,Q,|V|}$ are the standard uncertainties for each type of measurement. These uncertainties are calculated based on the maximum error of the smart meter accuracy class and assuming a 95% confidence interval [16],

$$\sigma_{P,Q,|V|} = \frac{e_{P,Q,|V|}}{1.96} \tag{1.b}$$

where $e_{P,Q,|V|}$ is the measurement device maximum errors defined by the accuracy class of the smart meters.

III. Modified WLS State Estimation

While various techniques have been developed for the monitoring of power systems [3], the WLS SE method is the most established and widely used. In this paper, the proposed monitoring scheme, in which the neutral voltage is included in the state vector, is also based on this technique. Since the choice

of the form of the state variables (current or voltage, polar or rect.) does not affect significantly the accuracy of the estimated results [3], the formulation of the proposed monitoring scheme is developed using the voltage magnitude and angle as state variables. Without losing generality, a similar approach can be followed for any other form of state variables in order to take into consideration the voltage of the neutral conductor.

A. Weighted Least Squares State Estimation

For a given set of system measurements, the state variables are calculated by minimizing the weighted sum of the measurement residual [17],

$$\min \sum_{i=1}^{n} \frac{[z_i - h_i(\boldsymbol{x})]^2}{\sigma_i^2} \tag{2.a}$$

where z_i is the i^{th} measurement from the measurement vector $\boldsymbol{z}$, $h_i(\boldsymbol{x})$ is the measurement function that relates the state variables with the i^{th} measurement, $\boldsymbol{x}$ is the state vector and σ_i is the standard deviation of the i^{th} measurement. As it can be seen from (2.a), the standard deviation of each measurement is used as a weight in order to give higher priority to measurements that are more accurate than other measurements.

Distribution grids are usually radial or slightly meshed, which has as a result a significant number of zero injection nodes. By exploiting this characteristic, PQ measurements can be constructed for these nodes. However, since there is no uncertainty behind these measurements, if they are included in the measurement vector $\boldsymbol{z}$ then effectively all other measurements will be ignored and the system will become ill-conditioned. Instead, the problem is formulated as an optimization problem with equality constraints [18]. By applying the Lagrange and then the Gauss-Newton method, the state vector is obtained by solving the below iterative scheme,

$$\begin{bmatrix} \Delta \boldsymbol{x} \\ \boldsymbol{\lambda} \end{bmatrix} = \begin{bmatrix} \boldsymbol{H}^T(\boldsymbol{x}^k)\boldsymbol{R}^{-1}\boldsymbol{H}(\boldsymbol{x}^k) & -\boldsymbol{C}^T(\boldsymbol{x}^k) \\ \boldsymbol{C}(\boldsymbol{x}^k) & \boldsymbol{0} \end{bmatrix}^{-1} \begin{bmatrix} \boldsymbol{H}(\boldsymbol{x}^k)\boldsymbol{R}^{-1}\Delta \boldsymbol{z}^k \\ -\boldsymbol{c}(\boldsymbol{x}^k) \end{bmatrix} \tag{2.b}$$

where k is the iteration number, $\Delta \boldsymbol{x} = \boldsymbol{x}^k - \boldsymbol{x}^{k+1}$, $\Delta \boldsymbol{z} = \boldsymbol{z} - \boldsymbol{h}(\boldsymbol{x}^k)$ and $\boldsymbol{R}$ is a diagonal matrix (assuming the measurement errors are uncorrelated [19]) containing the measurement variances ($R = diag\{\sigma_1^2, \sigma_2^2, \dots, \sigma_n^2\}$). The vector $\boldsymbol{c}(\boldsymbol{x})$ contains the nonlinear functions that relate the zero power injection measurements with the state variables, while $\boldsymbol{C}(\boldsymbol{x}) = \partial \boldsymbol{c}(\boldsymbol{x})/\partial \boldsymbol{x}$ and similarly $\boldsymbol{H}(\boldsymbol{x}) = \partial \boldsymbol{h}(\boldsymbol{x})/\partial \boldsymbol{x}$. This iterative process is repeated until the update vector $\Delta \boldsymbol{x}$ satisfies a predefined criterion. In this paper, the procedure is stopped when the maximum absolute value of the update vector is less than $\varepsilon = 10^{-4}$ and consequently (2.c) is satisfied,

$$\|\Delta \boldsymbol{x}^k\|_\infty = max\{|\Delta \boldsymbol{x}^k|\} < \varepsilon \tag{2.c}$$

B. Proposed Modifications

1) *A four phase system:* In the C_N for four-wire LVDGs, it is common to use Kron's reduction method in order to merge the neutral conductor with the phase conductors [5]-[6]. This allows to simplify the problem and treat the four-wire distribution grid as a three-wire system. However, the use of Kron's reduction method requires the assumption that the voltage across the neutral conductor approximates to zero. In the case of a four-wire LVDG in which the neutral conductor is grounded only at the transformer substation, this assumption is not valid, and its use can lead to inaccurate results [5]. As a matter of fact, in [14], it was shown that due to the significant zero-sequence current that flows through the neutral conductor (and consequently the voltage drop across it), the C_N yields inaccurate results. Therefore, in such LVDGs the use of Kron's reduction method should be avoided as the resulting system model will not be an accurate representation of the physical system. Instead, the full 4x4 impedance matrix (3.a) of each of the distribution lines should be used and the system should be modeled as a four-phase system. Hence, every four-wire node is characterized by eight state variables and every two-wire node by four state variables, as given by (3.b)-(3.c).

$$Z_{4x4} = \begin{bmatrix} z_{aa} & z_{ab} & z_{ac} & z_{an} \\ z_{ba} & z_{bb} & z_{bc} & z_{bn} \\ z_{ca} & z_{cb} & z_{cc} & z_{cn} \\ z_{na} & z_{nb} & z_{nc} & z_{nn} \end{bmatrix} \tag{3.a}$$

$$x_{abcn} = (\theta_a, \theta_b, \theta_c, \theta_n, |V_a|, |V_b|, |V_c|, |V_n|) \tag{3.b}$$

$$x_{pn} = (\theta_p, \theta_n, |V_p|, |V_n|) \tag{3.c}$$

2) *Measurement functions and Jacobian matrix:* In a LVDG, the main measuring equipment are smart meters which can provide the active-reactive power consumption of the consumers as well as voltage magnitude measurements. As aforementioned, smart meters provide phase-to-neutral measurements and therefore the measurement functions that are used in the WLS SE procedure must be adjusted accordingly. Firstly, the typical power injection measurements [5]-[6] for a three-phase analysis are modified to include the coupling with the neutral voltage,

$$P_i^p = |V_i^p| \sum_{k=1}^{N} \sum_{m=a}^{n} |V_k^m| \left(G_{ik}^{pm} cos\delta_{ik}^{pm} + B_{ik}^{pm} sin\delta_{ik}^{pm}\right) \tag{4.a}$$

$$Q_i^p = |V_i^p| \sum_{k=1}^{N} \sum_{m=a}^{n} |V_k^m| \left(G_{ik}^{pm} sin\delta_{ik}^{pm} - B_{ik}^{pm} cos\delta_{ik}^{pm}\right) \tag{4.b}$$

where P_i^p and Q_i^p is the injected active and reactive power respectively at node i in phase p, $\delta_{ik}^{pm} = \delta_i^p - \delta_j^m$, $\boldsymbol{Y} = \boldsymbol{G} + j\boldsymbol{B}$ is the admittance matrix of the system, $m = a, b, c, n$ corresponds to the system's phases and N is the total number of nodes in the system.

Secondly, since the voltage measurements are phase-to-neutral measurements, they cannot be directly related to the corresponding state variables as in the C_N SE. Instead, each phase-to-neutral voltage measurement is now related with four state variables as shown below,

$$\left|V_i^{p-n}\right| = \left|\left|V_i^p\right| \angle \theta_i^p - |V_i^n| \angle \theta_i^n\right| \tag{5.a}$$

$$\begin{aligned} \left|V_i^{p-n}\right| = \Big[&\left(\left|V_i^p\right| \cos\left(\theta_i^p\right) - |V_i^n| \cos\left(\theta_i^n\right)\right)^2 + \\ &\left(\left|V_i^p\right| \sin\left(\theta_i^p\right) - |V_i^n| \sin\left(\theta_i^n\right)\right)^2\Big]^{1/2} \end{aligned} \tag{5.b}$$

$$\left|V_i^{p-n}\right| = \sqrt{\left|V_i^p\right|^2 + \left|V_i^n\right|^2 - 2\left|V_i^p\right|\left|V_i^n\right| \cos\left(\theta_i^p - \theta_i^n\right)} \tag{5.c}$$

As it can be seen from the above expression, each voltage magnitude measurement is now related to the phase and neutral voltage magnitude and angle of the corresponding system node. Consequently, the relevant elements of the Jacobian matrix $\boldsymbol{H}(\boldsymbol{x})$ are modified accordingly,

$$\frac{\partial|V_i^{p-n}|}{\partial|V_j^m|}=\begin{cases}\dfrac{|V_j^m|-|V_i^n|\cos(\theta_j^m-\theta_i^n)}{h_{|V|}(\boldsymbol{x})}, & j=i,\quad m=p\\ \dfrac{|V_j^m|-|V_i^p|\cos(\theta_i^p-\theta_j^m)}{h_{|V|}(\boldsymbol{x})}, & j=i,\quad m=n\\ 0, & otherwise\end{cases} \tag{5.d}$$

$$\frac{\partial|V_i^{p-n}|}{\partial\theta_j^m}=\begin{cases}\dfrac{|V_j^m||V_i^n|\sin(\theta_j^m-\theta_i^n)}{h_{|V|}(\boldsymbol{x})}, & j=i,\quad m=p\\ -\dfrac{|V_i^p||V_j^m|\sin(\theta_i^p-\theta_j^m)}{h_{|V|}(\boldsymbol{x})}, & j=i,\quad m=n\\ 0, & otherwise\end{cases} \tag{5.e}$$

where $h_{|V|}(\boldsymbol{x})$ corresponds to the measurement function described in (5.c). In the C_N SE, in which the voltage measurements can be related directly to the state variables, the $\partial|V_i^p|/\partial|V_j^m|$ element of the Jacobian matrix $\boldsymbol{H}(\boldsymbol{x})$ is equal to 1 when $j=i$ and $m=p$ and equal to zero otherwise, while $\partial|V_i^p|/\partial\theta_j^m$ is always equal to zero.

3) *Virtual measurements for the neutral voltage:* It is well known that the use of the Gauss-Newton method to solve a set of nonlinear functions can have convergence issues related with the initialization point [20]. Usually, this is not a major problem in the C_N as the actual operating conditions are not very far from the initialization point as the system is regulated to operate near to its nominal values (usually the initialization point). However, by including the neutral voltage, which is normally initialized to 0 V, the convergence of the WLS can be deteriorated [13]. In such case, the neutral voltage might fluctuate between some values far from its initialization value. To improve the convergence capabilities when the neutral voltage is also considered, virtual measurements are constructed with the use of the forward-backward voltage sweep method (FBS) and the active-reactive power injection measurements. The term virtual measurements is used for differentiating from pseudo-measurements as a priori information is not required. Rather, the available knowledge from the smart meters (power measurements) is utilized to gain more information (neutral voltage) about the system's state, during the execution of the DSSE. This new information is then used as measurements in the proposed DSSE scheme with the purpose of guiding the estimation of the neutral voltage.

The general scheme of the FBS method is illustrated in Fig. 1. This method is an iterative procedure, in which in every iteration the load and branch currents are calculated using the PQ information of the loads, the grid topology and an initial guess (flat start) for the load voltages. In [21] the effect of different neutral conductor configurations on the methodology's convergence are examined. It is concluded that for certain configurations, multiple solutions might exist and

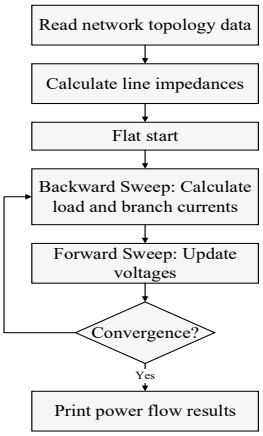

Fig. 1. FBS scheme

the convergence of the FBS depends on the initialization of the neutral voltage, while in some cases FBS fail to converge. However, for radial systems with the neutral grounded at the loads, FBS converges to the same solution, regardless of the initialization of the neutral voltage. This observation is extended in [22] for radial systems with the neutral grounded only at the transformer substation. Therefore, despite that the results of the FBS are characterized by a considerable uncertainty [12], they are still a good indication for the neutral voltage and can be used as virtual measurements in the proposed WLS SE. The FBS method used in this paper to construct the virtual measurements of the neutral voltage is the one described in [22]. The main difference of this method with other FBS methods [23] is that during the calculation of the load currents in the backward sweep, the neutral voltage is also considered,

$$\begin{bmatrix}I_a^i\\ I_b^i\\ I_c^i\\ I_n^i\end{bmatrix}=\left[\left(\frac{S_a^i}{(V_a^i-V_n^i)}\right)^*\left(\frac{S_b^i}{(V_b^i-V_n^i)}\right)^*\left(\frac{S_c^i}{(V_c^i-V_n^i)}\right)^*\sum_m I_m^i\right]^T \tag{6.a}$$

where $m=\{a,b,c\}$, i is the i^{th} node with a load, S_a^i, S_b^i and S_c^i is the power measurement of this load and V_a^i, V_b^i, V_c^i and V_n^i are the voltages of the i^{th} node. Once the FBS converges, the neutral voltage magnitude and phase angle are used as virtual measurements and are included in the measurement vector $\boldsymbol{z}$,

$$\boldsymbol{z}=[\,\boldsymbol{P_{inj}}\quad\boldsymbol{Q_{inj}}\quad|\boldsymbol{V}^{p-n}|\quad|\boldsymbol{V}^n|\quad\boldsymbol{\theta}^n\,]^T \tag{6.b}$$

The final form the of the Jacobian matrix $\boldsymbol{H}(\boldsymbol{x})$ is,

$$\boldsymbol{H}(\boldsymbol{x})=\begin{bmatrix}\dfrac{\partial\boldsymbol{P_{inj}}}{\partial\boldsymbol{\theta}} & \dfrac{\partial\boldsymbol{Q_{inj}}}{\partial\boldsymbol{\theta}} & \dfrac{\partial|\boldsymbol{V}^{p-n}|}{\partial\boldsymbol{\theta}} & \boldsymbol{0} & \dfrac{\partial\boldsymbol{\theta}^n}{\partial\boldsymbol{\theta}}\\ \dfrac{\partial\boldsymbol{P_{inj}}}{\partial|\boldsymbol{V}|} & \dfrac{\partial\boldsymbol{Q_{inj}}}{\partial|\boldsymbol{V}|} & \dfrac{\partial|\boldsymbol{V}^{p-n}|}{\partial|\boldsymbol{V}|} & \dfrac{\partial|\boldsymbol{V}^n|}{\partial|\boldsymbol{V}|} & \boldsymbol{0}\end{bmatrix}^T \tag{6.c}$$

IV. Weights For The Virtual Measurements

A. Normality Tests

In the C_N it is usually assumed that the measurement errors follow a normal distribution with a known variance and a zero mean value (i.e. $N(0,\sigma^2)$) [17]. Similarly, in this paper it is

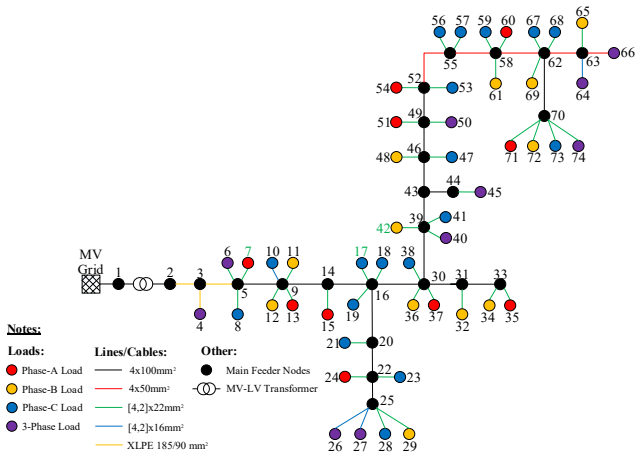

Fig. 2. The LVDG under consideration

assumed that the measurement error of the conventional measurements (P_{inj}, Q_{inj} and $|V^{p-n}|$) also follows a normal distribution. Therefore, in order to incorporate properly the virtual measurements in the proposed DSSE, a statistical analysis is necessary in order to identify the statistical distribution of their errors. Considering that for the calculation of the virtual measurements, the active and reactive power measurements are used, whose errors do follow a normal distribution, it is assumed that also the error of the virtual measurements follows a normal distribution (null hypothesis). Then, the Anderson-Darling [24] and Shapiro-Wilk [25] fitness tests are used to determine whether this hypothesis must be refuted. These fitness tests determine if the null hypothesis must be refuted by calculating the so-called *p-value* index. If this index is below 0.05 [26] then the hypothesis is refuted, and it cannot be assumed that the virtual measurements' error follows a normal distribution.

In Fig. 2, the LVDG that is considered in this paper is illustrated. It is assumed that all consumers are equipped with a smart meter belonging to the C-4 accuracy class (see Table II), more information about this system can be found in Section V. This system is implemented in MATLAB/Simulink where the power flow results of one time step represent the real state of the system and are used to create the measurement errors for P_{inj} and Q_{inj} using (1.a). FBS is executed 3000 times with different measurement errors, extracted by normal distributions with the appropriate properties. Then, the results are compared each time to the true state of the system in order to create the measurement error vector for each virtual measurement (72 $|\boldsymbol{V}^n|$ and 72 $\boldsymbol{\theta}^n$, one for each low voltage node). This measurement error vector is used as input to the two fitness tests which results to 144 p-values for $|\boldsymbol{V}^n|$ (72 from each fitness test) and 144 p-values for $\boldsymbol{\theta}^n$. All p-values are found to be well above the threshold of 0.05 and in Table III the average p-value of each type of virtual measurement is provided for each fitness test. Moreover, in Fig. 3 the probability density and probability plot of the $|\boldsymbol{V}^n|$ error is presented for a random system node. This figure offers a visual inspection of the distribution of the measurement error as it's compared to a fitted normal distribution [27]. From Fig. 3 and Table III it can be concluded that the null hypothesis is valid (based on these fitness tests). In other words, the assumption that the error of the virtual measurements follows a normal distribution holds true.

TABLE III
AVERAGE P-VALUES

Fitness test	p-value $\|\boldsymbol{V}^n\|$ (average)	p-value $\boldsymbol{\theta}^n$ (average)
Anderson-Darling	0.5475	0.2786
Shapiro-Wilk	0.6456	0.2173

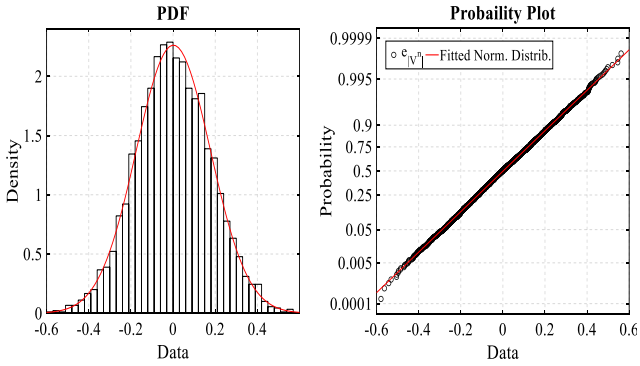

Fig. 3. Visual inspection of the normality of the virtual measurements

B. Measurement Weights

The matrix $\boldsymbol{R}$, as defined in Section III. A. is formulated using the variance of each measurement and its inverse ($\boldsymbol{R^{-1}}$) is utilized to weight each measurement used in the WLS estimator. Measurements with high uncertainty (high variance) have a low impact on the WLS SE as their corresponding weight is smaller in relation to more accurate measurements (low variance). For the virtual measurements, after verifying that their error follows a normal distribution, their uncertainty must be defined in order to properly incorporate them in the estimation procedure. To do so, two different strategies are followed to define their uncertainty. The first one (W_1) is a simple and straightforward while the second one (W_2) is more complex. The effect of the resulting calculated uncertainty of the virtual measurements in the WLS SE for each of the two procedures is examined in Section V.

1) W_1: Considering that the calculation of the virtual measurements is achieved through the measurements of the active and reactive power consumption, their uncertainties are directly related. Therefore, a straightforward calculation of the uncertainty of the virtual measurements can be the follow,

$$\sigma_{W_1} = \sqrt{\sigma_{P_{inj}}^2 + \sigma_{Q_{inj}}^2} \tag{7.a}$$

In Table IV, the calculated uncertainty of the virtual measurements for each of the smart meter accuracy classes that are considered in this paper is presented.

TABLE IV
UNCERTAINTY OF VIRTUAL MEASUREMENTS, W_1 SCHEME

Accuracy class	σ_{W_1} [%]
C1	0.283
C2	0.707
C3	1.118
C4	2.236
C5	2.828

2) W_2: In Fig. 4 a typical four-wire, ungrounded, distribution line is illustrated. Considering the coupling between the phases, the voltage at the receiving end is,

$$\begin{pmatrix} V_a \\ V_b \\ V_c \\ V_n \end{pmatrix} = \begin{pmatrix} V_A \\ V_B \\ V_C \\ V_N \end{pmatrix} - \begin{pmatrix} z_{aa} & \cdots & z_{an} \\ \vdots & \ddots & \vdots \\ z_{na} & \cdots & z_{nn} \end{pmatrix} \begin{pmatrix} I_a \\ I_b \\ I_c \\ I_n \end{pmatrix} \quad (8.a)$$

The neutral voltage is equal to,

$$V_n = V_N - z_{na}I_a - z_{nb}I_b - z_{nc}I_c - z_{nn}I_n \quad (8.b)$$

Considering that the neutral current can be written as the sum of the phase currents and by assuming that the off-diagonal terms of the impedance matrix are almost identical to simplify the problem, (8.b) can be re-written as,

$$V_n = V_N - c(I_a + I_b + I_c) \quad (8.c)$$

where $c \in \mathbb{C}$ and is equal to $c = z_{nn} + z_m$ (z_m is the mutual impedance between the conductors). The phase currents are calculated based on the downstream loads of the specific receiving end (node) as,

$$f = c \sum_{i=L} \left(I_a^i + I_b^i + I_c^i \right) \quad (8.d)$$

$$f = c \sum_{i=L} \left[\left(\frac{P_a^i + jQ_a^i}{V_a^i} \right)^* + \left(\frac{P_b^i + jQ_b^i}{V_b^i} \right)^* + \left(\frac{P_c^i + jQ_c^i}{V_c^i} \right)^* \right] \quad (8.e)$$

where L is the set containing all downstream loads, in relation with the specific receiving end. For simplicity, the voltage are assumed to be equal to their nominal values [12] and by considering the phase shift introduced by the transformer they are equal to,

$$V_a = 1pu\angle -30° = 0.87 - j0.5 = e - jd \quad (9.a)$$

$$V_b = 1pu\angle -150° = -0.87 - j0.5 = -e - jd \quad (9.b)$$

$$V_c = 1pu\angle 90° = j1 = jg \quad (9.c)$$

Expression (8.e) can now be written as,

$$f = c_2 \sum \begin{matrix} \left(eP_a^i - dQ_a^i - eP_b^i - dQ_b^i + gQ_c^i \right) + \\ j\left(eQ_b^i + gP_c^i - dP_b^i - eQ_a^i - dP_a^i \right) \end{matrix} \quad (10.a)$$

$$f = c_2(R + jX) \quad (10.b)$$

where c_2 is equal to,

$$c_2 = \frac{c}{|V|^2} = \frac{z_{nn} + z_m}{|V|^2} = Z_r + jZ_x \quad (10.c)$$

The terms R and X are derived through the sum of normal distributions with a known standard deviation. Based on the propagation of uncertainty, the uncertainty of these terms also follows a normal distribution with a standard deviation that is a function of the standard deviation of the power measurements. Using expressions (10.b) and (10.c), f is written as,

$$f = (Z_r R - Z_x X) + j(Z_r X + Z_x R) \quad (11.a)$$

$$f = F_R + jF_X \quad (11.b)$$

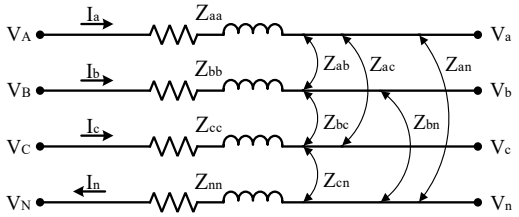

Fig. 4. A four-wire distribution line

where the uncertainty of each term can be calculated as,

$$\sigma_{F_R} = \sqrt{Z_r^2\sigma_R^2 + Z_x^2\sigma_X^2}\ , \quad \sigma_{F_X} = \sqrt{Z_r^2\sigma_X^2 + Z_i^2\sigma_R^2} \quad (11.c)$$

Now the neutral voltage can be written as,

$$V_n = V_N - f \quad (12.a)$$

$$V_n = \left(F_R^{V_N} - F_R^f\right) + j\left(F_X^{V_N} - F_X^f\right) \quad (12.b)$$

$$V_n = a + jb \quad (12.c)$$

where the uncertainty of a and b is calculated in a similar manner as in (11.a)-(11.c). The virtual measurements that will be used in the state estimation are calculated as,

$$|V_n| = \sqrt{a^2 + b^2} \quad (12.d)$$

$$\theta_n = \tan^{-1}(k) \quad (12.e)$$

where $k = b/a$. Considering the propagation of uncertainty, the uncertainty of each virtual measurement can be calculated as,

$$\sigma_{|V_n|} = \sqrt{\left(\frac{a}{|V_n|}\right)^2 \sigma_a^2 + \left(\frac{b}{|V_n|}\right)^2 \sigma_b^2} \quad (13.a)$$

$$\sigma_{\theta_n} = \frac{|k|}{1 + k^2} \sqrt{\left(\frac{\sigma_a}{a}\right)^2 + \left(\frac{\sigma_b}{b}\right)^2} \quad (13.b)$$

The calculation of the uncertainty of the virtual measurements is conducted in a forward sweep procedure. Considering that the neutral conductor is grounded at the transformer substation (at the second node), then $V_n^2 = 0$ and then according to (12.a) the rest are,

$$\begin{matrix} V_n^3 = V_n^2 - f^3 = -f^3 \\ V_n^4 = V_n^3 - f^4 = -f^3 - f^4 \\ V_n^5 = V_n^3 - f^5 = -f^3 - f^5 \\ \vdots \end{matrix} \quad (14.a)$$

In Fig. 5 the calculated uncertainty of each virtual measurement is illustrated for all the smart meter accuracy classes that are considered. As expected, the uncertainty of the virtual measurements when accurate smart meters are used is significantly lower than with lower quality meters.

Moreover, (13.a)-(13.b) correspond to the diagonal elements, related with the virtual measurements, of the covariance matrix $\boldsymbol{R}$. Since the virtual measurements for the neutral voltage are derived through the same power measurements, they are correlated and as a result the covariance matrix is not diagonal. Considering this correlation, the covariance matrix $\boldsymbol{R}$ is then,

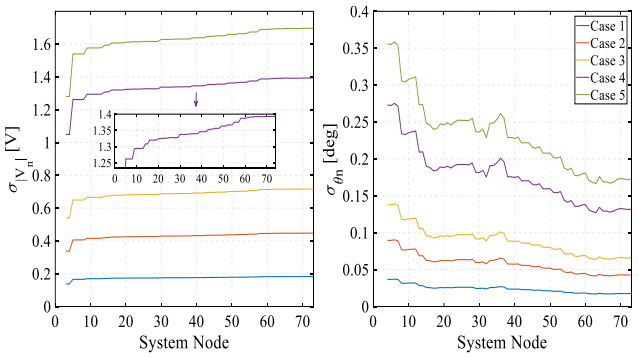

Fig. 5. Uncertainty of virtual measurements, W_2 scheme

$$R = \begin{bmatrix} \sigma_P^2 & 0 & 0 & 0 & 0 \\ 0 & \sigma_Q^2 & 0 & 0 & 0 \\ 0 & 0 & \sigma_{|V_{p-n}|}^2 & 0 & 0 \\ 0 & 0 & 0 & \sigma_{|V_n|}^2 & \sigma(|V_n|,\theta_n) \\ 0 & 0 & 0 & \sigma(\theta_n,|V_n|) & \sigma_{\theta_n}^2 \end{bmatrix} \quad (15.a)$$

where $\sigma(|V_n|,\theta_n)$ and $\sigma(\theta_n,|V_n|)$ is the correlation between the virtual measurements. For the calculation of this correlation, the power measurements from the smart meters at the load nodes are considered (first term of (8.c) is neglected) due to the high complexity. This is because the neutral voltage at the zero node before a load node is dependent on all the loads in the system. An analytical analysis of this will be too extensive for the potential improvement that it may offer. Considering this simplification, the neutral voltage at a load bus can be approximated as,

$$V_n \sim c_2 \begin{cases} (eP_a - dQ_a) - j(dP_a + eQ_a), & Phase\ A\ load \\ (-eP_b - dQ_b) + j(eQ_b - dP_b), & Phase\ B\ load \\ gQ_c + jgP_c\,, & Phase\ C\ load \\ (eP_a - dQ_a - eP_b - dQ_b + gQ_c) + & 3-Ph\ load \\ j(eQ_b + gP_c - dP_b - eQ_a - dP_a) & \end{cases} \quad (15.b)$$

In all cases, (15.b) can be written in polar form as,

$$V_n \sim |c_2| e^{j\theta_{c_2}} \sqrt{R^2 + X^2}\, e^{j \tan^{-1}\frac{X}{R}} \quad (15.c)$$

where R and X are the real and imaginary parts of (15.b) respectively. The virtual measurements can then be expressed as a function of the power measurements as follows,

$$|V_n| = |c_2|\sqrt{R^2 + X^2} \rightarrow f_{|V_n|}(P,Q) \quad (15.d)$$

$$\theta_n = \theta_{c_2} + \tan^{-1}\frac{X}{R} \rightarrow f_{\theta_n}(P,Q) \quad (15.e)$$

Using the propagation of uncertainty, the correlation between the virtual measurements is calculated as,

$$\sigma(|V_n|,\theta_n) = \sqrt{\sum\nolimits_{k=1}^{2} \left[\frac{\partial f_{|V_n|}}{\partial \boldsymbol{p}(k)} \frac{\partial f_{\theta_n}}{\partial \boldsymbol{p}(k)}\right] \left[\sigma(\boldsymbol{p}(\boldsymbol{k}))\right]^2} \quad (15.f)$$

where $\boldsymbol{p}(k) = [P, Q]$ are the active and reactive power measurements of the corresponding load and $\sigma(p) = [\sigma_P,\ \sigma_Q]$ is the uncertainty of these measurements.

V. Case Studies

In this section, the proposed monitoring scheme for ungrounded LVDGs is evaluated for both W_1 and W_2 weight schemes, referred to as N_{W_1} and N_{W_2} respectively. The system used in the simulations is illustrated in Fig. 2, which is an actual sub-urban residential LVDG in the power system of Cyprus. In total, there are 50 service points and 62 consumers, where most of them are supplied by a single phase and a small number have a three-phase connection. The three-phase load nodes 4 and 6 correspond to apartment complexes with 7 residents each. The aggregated consumption of these apartment complexes is considered in the case studies (full scale meter reading 30 kVA), therefore they are modeled as a single three-phase load. This LVDG has also 3 PV plants at nodes 7, 17 and 42 (denoted with a green font number) with rated power of 2.5 kWp, 7.35 kWp and 4.05 kWp respectively. The neutral conductor is grounded only at the 11 kV/ 433 V transformer substation, i.e. at node 2. Daily load profiles for each of the consumers have been constructed with a half-hourly resolution. This dataset was provided by the Cyprus DSO (Electricity Authority of Cyprus).

To properly evaluate the proposed monitoring scheme, the C_N SE is also considered in the simulations. Furthermore, the C_N is also applied to the same system, under the same operating conditions but with a multi-grounded neutral conductor (grounded at each end of a distribution line). The results of this simulation, referred to as C_{N^+}, represent the maximum performance of the traditional WLS SE and are valid only for a multi-grounded system. Since an ungrounded LVDG is considered, C_{N^+} is only used as a benchmark for the proposed monitoring scheme.

The operation of the LVDG is simulated for 5 days in MATLAB/Simulink to obtain the true values of the system's states. Based on the considered accuracy class of the smart meters, the conventional measurements are then constructed by adding a Gaussian noise. The performance of the monitoring schemes is evaluated by calculating the average 2-norm $\|\Delta V\|_2$ and max-norm $\|\Delta V\|_\infty$ of the voltage estimation error at each time step.

A. Accuracy class of the smart meters

In Fig. 6 the voltage estimation errors are illustrated for the C-4 smart meter accuracy class. It can be observed that the proposed monitoring scheme with the W_1 weights is considerably more accurate compared to the C_N. As it was shown in [14], the performance of C_N is highly affected by the zero-sequence current that is flowing in the system and therefore depends on the operating conditions. In N_{W_1}, since the neutral voltage is considered in the problem formulation, its performance not only is 6 times higher (in average) than C_N but also significantly more stable as its affected by the operating conditions in a considerably lower degree. The performance of the proposed monitoring scheme is further enhanced when the W_2 weights are used. Under this weight scheme for the virtual measurements, the performance of the proposed monitoring scheme approaches the maximum performance of the traditional WLS SE, highlighting the significance of properly assigning the weights for the virtual measurements. It should be

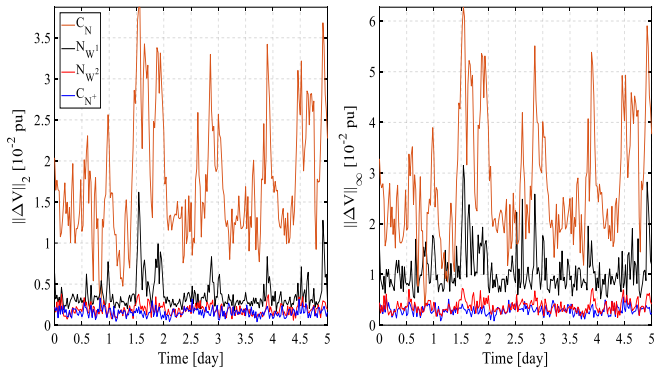

Fig. 6. Voltage estimation errors

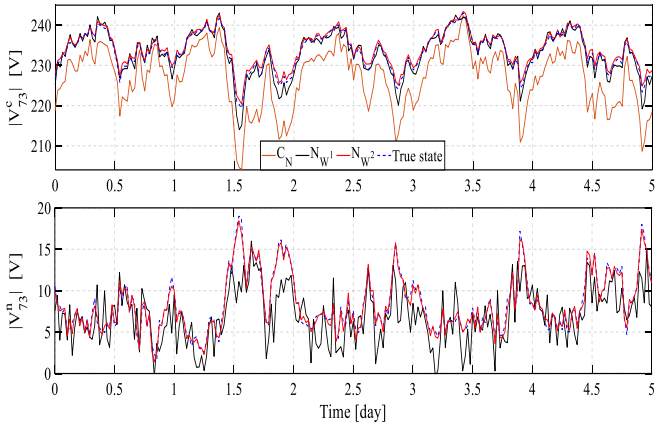

Fig. 7. Voltage profile estimation of node 73, different monitoring scheme

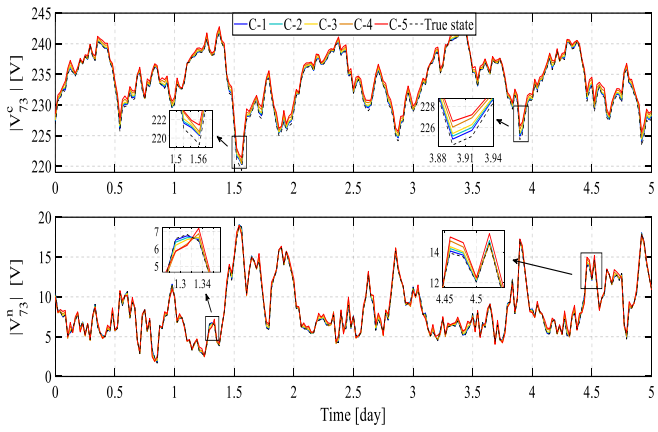

Fig. 8. Voltage profile estimation of node 73, different accuracy classes

noted that compared to C_{N^+}, the proposed monitoring scheme operates under a higher uncertainty. This is due to the neutral voltage whose virtual measurements are derived through erroneous PQ measurements and therefore as expected, its performance is lower than C_{N^+}. However, with the proper weights for the virtual measurements the proposed monitoring scheme achieves almost a similar performance while simultaneously it can estimate the neutral voltage without any additional measurements from the physical system.

In Fig. 7 the estimation of the voltage profile of node 73 is illustrated for the C-4 accuracy class and for the different monitoring schemes. This node was chosen since in average, the max-norm ($\|\Delta V\|_\infty^i$) of the estimation error originated from this node. From this figure, the improvement that the proposed

TABLE V
SUMMARY OF RESULTS, CONVENTIONAL MONITORING SCHEME

Case	C_N			C_{N^+}		
	Estimation errors [10^{-3} pu]		Average iterations	Estimation errors [10^{-3} pu]		Average iterations
	$\|\Delta V\|_2$	$\|\Delta V\|_\infty$		$\|\Delta V\|_2$	$\|\Delta V\|_\infty$	
1	19.61	30.77	3.29	0.17	0.38	3.19
2	19.63	30.82	3.29	0.51	1.03	3.20
3	19.66	30.85	3.30	0.82	1.61	3.20
4	19.71	30.96	3.32	1.58	3.01	3.19
5	20.21	31.64	3.35	2.55	4.32	3.19

TABLE VI
SUMMARY OF RESULTS, PROPOSED MONITORING SCHEME

Case	N_{W_1}			N_{W_2}		
	Estimation errors [10^{-3} pu]		Average iterations	Estimation errors [10^{-3} pu]		Average iterations
	$\|\Delta V\|_2$	$\|\Delta V\|_\infty$		$\|\Delta V\|_2$	$\|\Delta V\|_\infty$	
1	0.75	2.29	3.45	0.51	1.80	3.22
2	1.38	3.74	3.80	0.73	1.82	3.21
3	2.32	6.17	4.27	1.01	2.25	3.24
4	3.95	11.21	4.97	1.93	3.77	3.26
5	4.82	14.02	5.4	2.66	4.95	3.26

DSSE offers over the C_N in the voltage profile estimation can be clearly observed. In particular, the estimated states from N_{W_2} are always significantly closer to the true states. Moreover, N_{W_2} can also estimate accurately the neutral voltage of the system. Comparing Fig. 6 and 7 it can be concluded that the peaks of the estimation error of C_N happen when the neutral voltage reaches a significant value, i.e. at $t \approx 1.6$ days. At these time instances the neutral voltage has a significant value. The two main factors behind this considerable estimation error is the use of Kron's reduction, which results to an inaccurate system model, and the voltage measurements, which are all expressed with significantly different reference points. In comparison, in the proposed DSSE since the use of Kron's reduction is avoided, the voltage measurements are expressed as phase-to-neutral measurements and the neutral voltage is considered as a state variable, its performance is not affected by the operational state of the neutral voltage.

In Fig. 8, the estimation of the voltage profile of the same node is illustrated for the various smart meter accuracy classes using the N_{W_2}. While its accuracy is affected by the quality of the smart meters, even under the worst scenario the proposed monitoring scheme can still estimate fairly accurate the voltage profile. This shows the robustness of the proposed monitoring scheme as its performance is not greatly affected by the operating conditions nor by the quality of the smart meters.

In Table V-VI the average estimation errors (of the 5 days simulated) as well as the average iterations required for all monitoring schemes and for all smart meter accuracy classes are provided. In all cases the proposed DSSE with both weight schemes (N_{W_1} and N_{W_2}) achieves a considerably higher performance compared to C_N. Regarding the number of iterations required by the DSSE in order to converge, the weight scheme N_{W_2} improves significantly the computational performance of the proposed DSSE. In all case studies, the proposed DSSE with the N_{W_2} weight scheme required an average number of iterations slightly higher than 3, which is similar with the computational performance of the benchmark.

B. Type of system

In [14], the performance of C_N was evaluated under different types of LVDGs. It was identified that its performance was highly affected by the type of LVDG, where rural systems imposed higher estimation error. To validate the applicability of the proposed DSSE, different types of LVDGs are considered. The results of this case study are illustrated in Table VII, where case L corresponds to the original line lengths for the system's distribution lines.

Using the proposed DSSE, the accuracy of the estimation results remains fairly constant and very similar with C_{N^+}, regardless of the system type. On the contrary, the accuracy of C_N is highly affected by the system type, where, as in [14], rural systems impose higher estimation error. The main reason for this is the overall higher line impedance in rural systems, which for the same zero-sequence current as in an urban system, it results to a significantly higher neutral voltage. Consequently, the use of Kron's reduction in such systems results to a system model that is completely wrong. The higher neutral voltage in rural systems also affects in a greater degree the voltage measurements from the smart meters. Across a rural system, the neutral voltage from one node to another is significantly different, meaning that the reference point of each voltage measurement is also significantly different. In the proposed DSSE, all these issues are addressed with the proposed modifications and the developed weight scheme for the virtual measurements. As a result, the proposed DSSE can be applied to any type of LVDG without a significant change in its performance.

TABLE VII
SUMMARY OF RESULTS, DIFFERENT TYPES OF A LVDG

Case	C_N		C_{N^+}		N_{W_2}	
	Estimation errors [10^{-3} pu]		Estimation errors [10^{-3} pu]		Estimation errors [10^{-3} pu]	
	$\|\Delta V\|_2$	$\|\Delta V\|_\infty$	$\|\Delta V\|_2$	$\|\Delta V\|_\infty$	$\|\Delta V\|_2$	$\|\Delta V\|_\infty$
Urban 0.5L	10.97	15.45	1.53	2.57	1.84	2.87
0.75L	15.65	22.78	1.55	2.79	1.91	3.29
L	19.71	30.96	1.58	3.01	1.93	3.77
1.25L	23.34	36.71	1.66	3.25	2.12	4.37
Rural 1.5L	29.73	46.89	1.71	3.5	2.38	5.25

C. Monte Carlo trials

To unbias the results from the random measurement errors and to calculate their uncertainty, Monte Carlo simulations are conducted for N_{W^2}, using the C-4 smart meter accuracy class. The IEEE European low voltage test feeder, Fig. 9, is consider which is a significantly larger system than the LVDG in Cyprus. From this system, 50 different operational points are used for the Monte Carlo analysis. For each operational point, 3000 trials are executed using the proposed DSSE, considering different measurement errors in each trial, resulting in a total of 150 000 Monte Carlo trials. The mean and variance of each measurement error are provided in Table VIII.

A significant advantage of the proposed DSSE is that the convergence issues that are related with the initialization of the neutral voltage [13] are eliminated. The proposed DSSE, despite including the neutral voltage as a state variable, was able to converge in all the 150 000 Monte Carlo trials. In order

TABLE VIII
MONTE CARLO RESULTS

Estimation error	μ [V]	σ^2 [V^2]
$\|\Delta V\|_2$	0.293	0.012
$\|\Delta V\|_\infty$	0.570	0.042

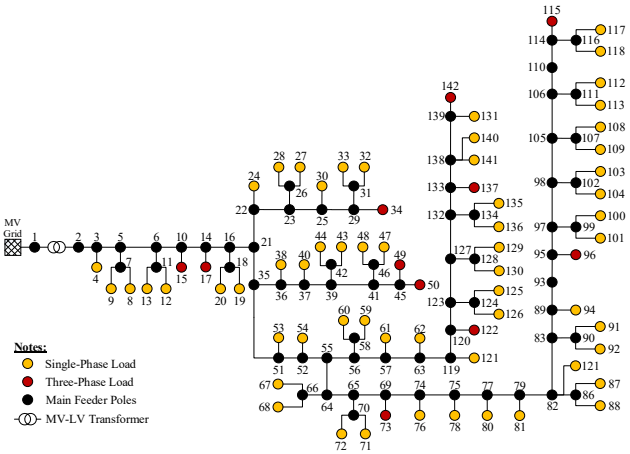

Fig. 9. IEEE European low voltage test feeder

to highlight the importance of the proposed modifications to the convergance rate of the DSSE, the following scenario is executed: The performance of the DSSE with the neutral voltage included in the state vector but without the proposed modifications regarding the virtual measurements is examined. During this scenario, the initial convergence threshold ε, equation (2.c), is set to 5×10^{-4} p.u. If the DSSE fails to converge within 30 iterations, then ε is increased by $+5 \times 10^{-4}$ p.u. If ε reaches 0.1 p.u and the DSSE still fails to converge then the process is stopped as the DSSE failed to converge within a reasonable convergence threshold.

The results of this study are illustrated in Fig. 10. The right axis with the red circles shows the required threshold setting in each of the operational points for the DSSE to achieve convergence and the left axis shows the required number of iterations for this threshold setting. In total there are 11 instances where the upper limit of ε was reached and the DSSE still failed to converge within 30 iterations. For comparison purposes, in Fig. 11 the required convergence threshold and number of iterations of the proposed DSSE with the virtual measurements is illustrated. With the inclusion of the proposed modifications and virtual measurements, the DSSE becomes

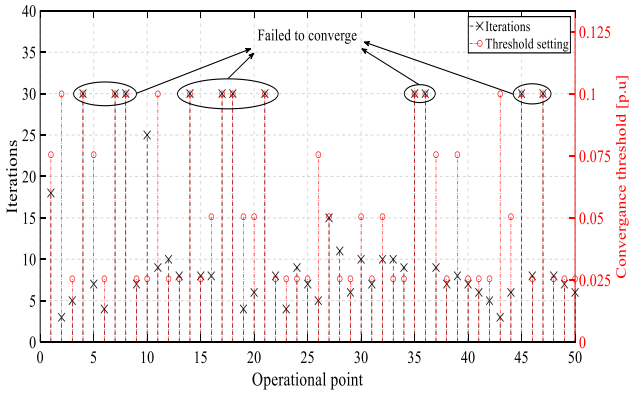

Fig. 10. DSSE convergence without virtual measurements

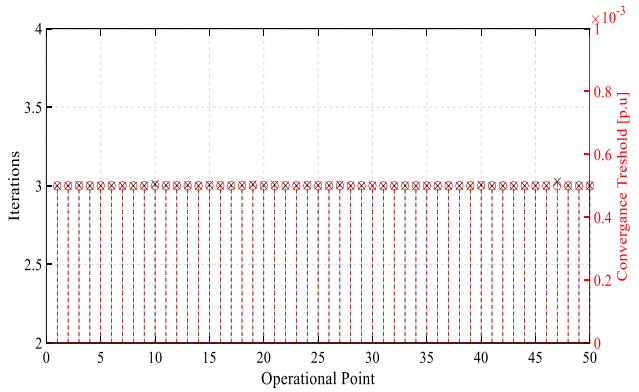

Fig. 11. Proposed DSSE convergence with virtual measurements

significantly more stable. Based on these numerical simulations, the proposed DSSE can achieve convergence in the lowest threshold setting and in average within 3 iterations. When the virtual measurements are not considered, the threshold limit must be considerably larger in order to achieve convergence, where in some instances no convergence can be achieved. This highlights the importance of the proposed modifications to the DSSE scheme when the neutral voltage is considered as a state variable.

VI. Conclusions

Current DSSE methods for MVDGs are not applicable in LVDGs with a neutral conductor grounded only at the MV-LV substation. This paper presented a novel monitoring scheme, based on the WLS SE, for such systems. In the proposed DSSE, the neutral voltage is included in the state vector, the measurement functions and the Jacobian matrix $\boldsymbol{H}(\boldsymbol{x})$ are adjusted accordingly and virtual measurements are incorporated in the WLS procedure. The purpose of the virtual measurements is to address any potential convergence issues and to improve the accuracy of the proposed DSSE. Case studies under different operating conditions and smart meter accuracy classes have demonstrated the effectiveness of the proposed monitoring scheme. In comparison to the conventional DSSE, in which the neutral voltage is assumed that it can be approximated to zero voltage, the proposed scheme has in average 10 times better performance. Further, when compared to the benchmark (maximum performance of the conventional DSSE) the performance of the proposed scheme is in average only 1.22 times lower, despite operating under higher uncertainty. As the case studies have illustrated, the proposed DSSE can operate with very high accuracy, which is not affected by the quality of the smart meters (case study A), the type and size of the LVDG (case study B) and the ungrounded neutral. With the introduction of the virtual measurements and the developed weight scheme, the proposed DSSE is also able to achieve convergence (case study C), something which was lacking when the neutral voltage was considered as a state variable before.

References

[1] G.T. Heydt, "The next generation of power distribution systems," *IEEE Trans. Smart Grid,* vol. 1, no. 3, pp. 225-235, Dec. 2010.

[2] K. Dehghanpour, Z. Wang, J. Wang, Y. Yuan and F. Bu, "A survey on state estimation techniques and challenges in smart distribution systems," *IEEE Trans. Smart Grid,* vol. 10, no. 2, pp. 2312-2322, March 2019.

[3] A. Primadianto and C. N Lu, "A review on distribution system state estimation," *IEEE Trans. Power Systems,* vol. 32, no. 5, pp. 3875-3883, Sept. 2017.

[4] N. Uribe-Perez, L. Hernandez, D. Vega and I. Angulo, "State of the art and trend review of smart metering in electricity grids," in *Applied Sciences*, vol. 6, no. 68, pp. 1-24, Feb. 2016.

[5] C. Lu, J. H. Teng and W.-H. Liu, "Distribution system state estimation," *IEEE Trans. Power Systems,* vol. 10, no. 1, pp. 229-240, Feb. 1995.

[6] W. H. Kersting, *Distribution System Modeling and Analysis,* CRC Press, Boca Raton, FL, 2007.

[7] M. Pau, P. A. Pegoraro and S. Sulis, "Efficient branch-current based distribution system state estimation including synchronized measurements," *IEEE Trans. Instrum. Meas.,* vol. 62, no. 9, pp. 2419-2429, Sept. 2013.

[8] I. Dzafic, R. A. Jabr, I. Huseinagic and B. C. Pal, "Multi-phase state estimation featuring industrial-grade distribution models," *IEEE Trans. Smart Grid,* vol. 8, no. 2, pp. 609-618, March 2017.

[9] A. Alimardani, F. Therrien, D. Atanackovic, J. Jatskevich and E. Vaahedi, "Distribution system state estimation based on nonsynchronized smart meters," *IEEE Trans. Smart Grid,* vol. 6, no. 6, pp. 2919-2928, Nov. 2015.

[10] M. Pau, F. Ponci, A. Monti, S. Sulis, C. Muscas and P. Pegoraro, "An efficient and accurate solution for distribution system state estimation with multiarea architecture," *IEEE Trans. Instrum. Meas.,* vol. 66, no. 5, pp. 910-919, May. 2017.

[11] C. Muscas, S. Sulis, A. Angioni, F. Ponci and A. Monti, "Impact of different uncertainty sources on a three-phase state estimator for distribution networks" *IEEE Trans. Instrum. Meas.,* vol. 63, no. 9, pp. 2200-2209, Sept. 2014.

[12] M. Pau, E. Patti, L. Barbierato, A. Estebsari, E. Pons, F. Ponci and A. Monti, "Design and accuracy analysis of multilevel state estimation based on smart metering infrastructure," *IEEE Trans. Instrum. Meas.,* Jan. 2019.

[13] Y. Liu, J. Li and L. Wu, "State estimation of three-phase four-conductor distribution systems with real-time data from selective smart meters," in *IEEE Trans. Power Systems*, vol. 34, no. 4, pp. 2632-2643, July 2019.

[14] A. Kotsonias, L. Hadjidemetriou, M. Asprou and E. Kyriakides, "Performance investigation of a monitoring scheme for low voltage grids with a single grounded neutral," *IEEE PowerTech*, Milan, Italy, 2019.

[15] Y. Wang, Q. Chen, T. Hong and C. Kang, "Review of smart meter data analytics: applications, methodologies, and challenges," *IEEE Trans. Smart Grid,* vol. 10, no. 3, pp. 3125-3148, May 2019.

[16] JGCM: Evaluation of the measurement data-Guide to the expression of uncertainty in measurements, JGCM100, 2008.

[17] A. Abur and A. G. Exposito, *Power System State Estimation. Theory and Implementation.* New York, NY, USA: Marcel Dekker, 2004.

[18] W. Lin and J. Teng, "State estimation for distribution systems with zero-injection constraints," *IEEE Trans. Power Systems,* vol. 11, no. 1, pp. 518-524, Feb. 1996.

[19] E. Caro, A. J. Conejo and R. Minguez, "Power system state estimation considering measurement dependencies," *IEEE Trans. Power Systems,* vol. 24, no. 4, pp. 1875-1885, Nov. 2009.

[20] J. E. Dennis Jr., R. B. Schnabel, "Numerical methods for unconstrained optimization and nonlinear equations." in *Classics in Applied Mathematics, Society for Industrial and Applied Mathematics,* 1996

[21] L. Araujo, D. R. R. Penido, S. Carneiro Jr. and J. L. R. Pereira, "A study of neutral conductors and grounding impacts on the load flow solutions of unbalanced distribution systems," *IEEE Trans. on Power Systems*, vol. 31, no. 5, pp. 3684-3692, Sep. 2016.

[22] A. Kotsonias, L. Hadjidemetriou and E. Kyriakides, "Power flow for a four-wire radial low voltage distribution grid with a single point grounded neutral," in *Proc. IEEE ISGT*, Bucharest, Romania, 2019.

[23] R. M. Ciric, A. O. Feltrin and L. F. Ochoa, "Power flow in four-wire distribution networks – General Approach," *IEEE. Trans. Power Systems*, vol. 18, no. 4, pp. 1283-1290, Nov. 2003.

[24] T. W. Anderson and D.A. Darling, "A test of goodness of fit," in *Journal of the American Statist. Assoc.*, vol. 49, no. 268, pp. 765-769, 1954.

[25] S. S. Shapiro and M. B. Wilk, "An analysis of variance for normality (complete samples)," in *Biometrika*, vol. 52, no. 3-4, pp. 591-611, 1965.

[26] G. V. Dallal, Ed., *The Little Handbook of Statistical Practice.* Boston, MA, USA: Tufts University, 1999.

[27] A. Ghasemi and S. Zahediasl, "Normality tests for statistical analysis: A guide for non-statisticians," in *Int. J Endocrinol Metab.* pp. 486-489, 2012